JOURNAL OF GEOPHYSICAL RESEARCH, VOL. 87, NO. B7, PAGES 5422-5432, JULY 10, 1982

ANALYSIS OF LONG-PERIOD SEISMIC WAVES EXCITED BY THE MAY 18, 1980, ERUPTION OF MOUNT ST. HELENS - A TERRESTRIAL MONOPOLE?

Hiroo Kanamori and Jeffrey W. Given

Seismological Laboratory, California Institute of Technology, Pasadena, California 91125

Abstract. Long-period (100 to 260 s) Love and Rayleigh waves excited by the eruption of Mount St. Helens on May 18, 1980, and recorded by IDA, SRO, and ASRO stations were analyzed to determine the mechanism of the eruption. The amplitude radiation patterns of both Rayleigh and Love waves are two lobed with a nodal direction in E5°S for Rayleigh waves and in N5°E for Love waves. These radiation patterns preclude any double-couple mechanism. The radiation pattern, the initial phase, the relatively large amplitude ratio of Love to Rayleigh waves and the existence of clear nodes in the radiation patterns of fundamental mode and higher-mode Rayleigh waves suggest that the source is represented by an almost horizontal (less than 15° from the horizontal) single force pointed toward S5°W. The surface wave spectra fall off very rapidly at periods shorter than 75 s suggesting a very slow source process. Although the details of the source time history could not be determined, a smooth bell-shaped time function: $f_o s(t) = (1/2)f_o(1-\cos(\frac{t}{\tau}\pi))$ for $0 \leq t \leq 2\tau$ and $f_o s(t) = 0$ for $t \geq 2\tau$, with $\tau = 75$ s is considered appropriate on the basis of comparison between synthetic and observed seismograms and of the shape of the source spectrum. The peak value of the force f_o is about 10^{18} dynes. The tailing end of the source time function could not be resolved, and some overshoot may be added. The magnitude and the time history of the force can be explained by a northward landslide followed by a lateral blast observed at the time of the eruption. Two distinct events about 110 s apart can be identified on body wave and short-period surface wave records. The first event may correspond to the earthquake which triggered the landslide and the lateral blast. The second event appears to correspond to a second large earthquake and explosion which took place about 2 minutes after the first earthquake.

1. Introduction

The eruption of Mount St. Helens (crater coordinates: 46.2°N; 122.2°W) on May 18, 1980, excited long-period (100 to 260 s) seismic waves, and high-quality digital seismograms were recorded at many IDA (International Deployment of Accelerographs), SRO (Seismic Research Observatory), and ASRO (Abbreviated SRO) stations. These are probably the first data of this kind obtained for a volcanic event and provide a unique opportunity to study the physical mechanism of volcanic eruption.

In this paper we report the results of detailed analyses of Rayleigh and Love waves excited by this eruption. Since the elastic response of the earth is very accurately known, we can retrieve the source parameters of this unique event from observations at far-field. We will show that the source can be represented by a nearly horizontal single force pointed in S5°W direction.

Paper number 2B0401.
0148-0227/82/002B-0401 $05.00

2. Data

Table 1 lists the stations which recorded the surface waves excited by the eruption of Mount St. Helens. The seismograms are extracted from the original IDA, SRO, and ASRO tapes starting from the approximate origin time of an $m_b = 4.7$ ($M_S = 5.2$) event reported by the National Earthquake Information Service (NEIS) (hypocenter: 46.214°N, 122.194°W; d = 4 km, origin time: 1532:11 UT, May 18, 1980).

For the convenience of spectral analysis, an antialias filter with a cut-off period of 30 s described by Kanamori and Stewart [1976] is first applied to the long-period components of the SRO and ASRO seismograms. The records are then decimated at 10-s intervals. The two horizontal components are rotated into the radial and transverse components to isolate Love waves.

Several representative seismograms are shown in Figure 1. In general, Love waves are larger than Rayleigh waves. Also, at some stations (e.g., MAJ in Figure 1), Rayleigh wave R_2 is hardly visible, indicating that the Rayleigh wave radiation pattern has distinct nodes. Another important feature is that the observed surface waves are deficient in relatively short-period (less than 75 s) energy compared with those of ordinary earthquakes. For comparison, some seismograms of the Mammoth Lakes, California, earthquake of May 25, 1980, are shown in Figure 2. The absence of short-period energy and the enhancement of long-period energy in the record of Mount St. Helens eruption is obvious, indicating that the source process associated with the eruption is much slower than that of ordinary earthquakes.

3. Analysis and Interpretation

The analysis method is identical to that described by Kanamori and Given [1981]. We first window the fundamental mode Rayleigh waves R_i (i = 1, 2, 3, ...) and Love waves G_i (i = 1, 2, 3, ...) from the seismograms, Fourier transform them and then correct for geometrical spreading, attenuation, propagation phase delay, polar phase shift, and instrument response to obtain the source spectrum $\hat{V}_r$ and $\hat{V}_\phi$ for Rayleigh and Love waves, respectively. The expressions for $\hat{V}_r$ and $\hat{V}_\phi$ are given by equations (6) and (14) of Kanamori and Given [1981].

In Figure 3 the amplitude and phase spectra of $\hat{V}_r$ and $\hat{V}_\phi$ thus obtained are shown as a function of azimuth (measured clockwise from the north) at five periods, 256, 200, 150, 120, and 100 s. The phase spectrum is computed only at 256 s where the correction for the propagation phase delay is considered accurate. Figure 3 shows three important features:

TABLE 1. Stations and Phases used for the Analysis

Station	Network	Δ,deg	φ,deg	ϕ_B,deg	Phase
GAR	IDA	94.4	350	9	R_1, R_2
CMO	IDA	23.4	332	131	R_1
NNA	IDA	70.8	132	328	R_1
KON	ASRO	67.4	24	326	R_1, R_2, G_1, G_2
GRF	SRO	76.2	29	327	R_1, R_2, G_1, G_2
SNZ	SRO	103.7	224	40	R_1, R_2
CTA	ASRO	105.3	257	46	R_1, R_2, G_1, G_2
NWA	SRO	133.3	265	55	G_1, G_2
BOC	SRO	58.7	120	323	R_1, R_2
ZOB	ASRO	79.0	128	325	R_1, R_2, G_1, G_2
MAJ	ASRO	70.5	303	47	R_1, R_2, G_1, G_2
CHT	SRO	105.4	320	28	R_1, R_2, G_1, G_2
TAT	SRO	88.7	306	39	G_1

1. The Rayleigh-wave radiation pattern is two lobed with nodes in the azimuth of approximately 95° and 275° (i.e., E5°S and N85°W). The Love wave radiation pattern is also two lobed but rotated by 90° relative to that of the Rayleigh waves.

2. For both Love and Rayleigh waves, the spectrum is antisymmetric with respect to the epicenter; i.e., there is a phase difference of about 180° between the stations in opposite azimuths.

3. The amplitude of the Love waves is about twice as large as the Rayleigh-wave amplitude.

Observations 1 and 2 immediately preclude any double-couple mechanism for the source. For a shallow, double-couple source, Love wave radiation pattern is always four lobed [see e.g., Kanamori, 1970, Figure 4] except for a vertical dip slip source which has no seismic radiation when the source is very shallow. Also, for a double-couple source, the spectra at two stations in opposite azimuths are complex conjugate to each other.

Observation 3 favors a single force over any force dipoles without moment. Force dipoles generate Rayleigh waves more efficiently than Love waves. Furthermore, the large Love waves indicate that if the source is to be represented by a single force, it is more horizontal than vertical. A vertical force generates only Rayleigh waves.

With these observations in mind, we interpret the data using normal mode theory. Starting from *Saito's [1967] results and using the notation* by Kanamori and Cipar [1974] and Kanamori and Stewart [1976], we write the transverse component of the displacement of torsional oscillations due to a unit step function single force as

$$U_\phi(\vec{r},t) = \sum_n r_s L_2 \cos\alpha \sin\phi \frac{dP_n^1}{d\theta} \cos\omega_n t \qquad (1)$$

where α is the angle between the force and the horizontal (measured upward), r_s is the radial distance to the source from the center of the earth, L_2 is the excitation function defined by Kanamori and Cipar [1974], φ is the azimuth of the station measured counterclockwise from the azimuth of the horizontal projection of the force, ω_n is the eigen angular frequency, and the summation is over the modes. Using the asymptotic expansion of P_n^ℓ, and applying the various corrections for the propagation effects and the instrument response, we can write the source spectrum of Love waves which corresponds to $V_\phi(\omega)$ as

$$\hat{V}_\phi(\omega) = \left\{-i \cos\alpha \sin\phi \frac{r_s}{N} P_L^{(1)}\right\} \qquad (2)$$

$$N = \omega R/C - 1/2$$

where N is the order number of the mode having the angular frequency ω, C is the phase velocity, and R is the earth's radius. $P_L^{(1)}$ is the excitation function tabulated by Kanamori and Given [1981]. If the source is not a unit step function but is given by $f_o s(t)$ with its transform $f_o \hat{s}(\omega)$, $V_\phi(\omega)$ in (2) should be multiplied by $i\omega f_o \hat{s}(\omega)$.

Similar expressions are obtained for the vertical component of spheroidal oscillations and Rayleigh waves. Corresponding to (1) and (2), we obtain

$$U_r(\vec{r},t) = \sum_n r_s K_2 \left[-\frac{y_1(r_s)}{y_3(r_s)} \sin\alpha P_n^o - \cos\alpha\cos\phi P_n^1\right] \qquad (3)$$

$$\hat{V}_r(\omega) = \frac{r_s P_R^{(1)}}{N}\left[\frac{\sin\alpha}{N}\frac{y_1(r_s)}{y_3(r_s)} + i\cos\alpha\cos\phi\right] \quad (4)$$

In the above, $P_R^{(1)}$ is the excitation function of Rayleigh waves and is tabulated by Kanamori and Given [1981]. The term $y_1(r_s)/Ny_3(r_s)$ is approximately equal to the ratio of the vertical to horizontal components of the particle motion of Rayleigh waves at the surface and is about -1.5 for fundamental modes.

For an isotropic source (three mutually orthogonal dipoles without moment) given by $M_o s_M(t)$, we have

$$\hat{V}_r(\omega) = i\omega M_o \hat{s}_M(\omega) N_R^{(1)} \quad (5)$$

where $N_R^{(1)}$ is the excitation function defined by Okal [1978] and Kanamori and Given [1981]. For a shallow event, $P_L^{(1)} = -3.2$, $P_R^{(1)} = 1.7$, and $N_R^{(1)} \simeq -2/3\ P_R^{(1)} = -1.1$ at the period of 256 s (see the appendix of Kanamori and Given [1981] and Okal [1978]).

Figure 4 schematically shows the radiation patterns of Love and Rayleigh waves for a horizontal force, a vertical force, and an isotropic source computed by (2), (4), and (5). The absolute amplitude is arbitrary, but the relative amplitude is scaled properly for a period of 256 s. The moment of the isotropic source M_o is set equal to $M_o = f_o \cdot r_s / N$. The absolute phase is arbitrary, and only changes in the phase as a function of the azimuth are schematically shown. Comparison of Figure 4 with Figure 3

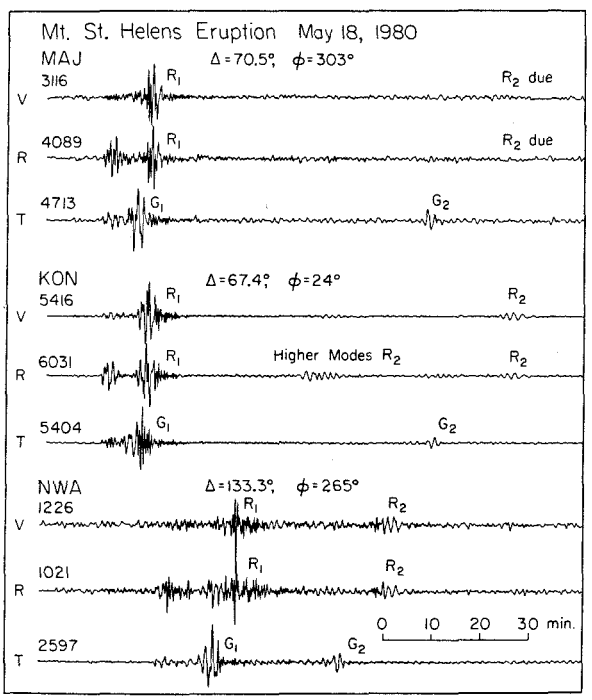

Fig. 1. Three-component seismograms of the eruption of Mount St. Helens at MAJ, KON, and NWA. Original seismograms are high-cut filtered at 30 s and rotated to vertical, radial, and transverse components. The beginning of the record is at 1532:11 UT, May 18, 1980. The peak-to-peak amplitude is given in digital counts.

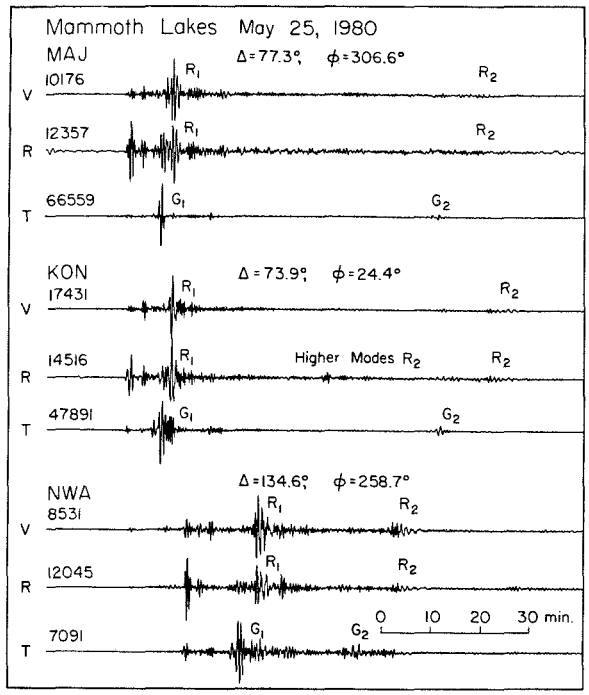

Fig. 2. Three-component seismograms of the Mammoth Lakes, California, earthquake of May 25, 1980, processed in the same way as those shown in Figure 1. Note the difference in the frequency content between the records of Mount St. Helens eruption and the Mammoth Lakes earthquake.

immediately suggests that a horizontal force pointed toward either north or south is appropriate to explain the observed radiation pattern. The source may have some vertical and/or isotropic component, but their combined effect should be small.

We make a more quantitative analysis in the following. Rewriting (3) for a source $f_o s(t)$, we have

$$\hat{V}_\phi = \frac{r_s P_L^{(1)}}{N}\omega\hat{s}(\omega) f_o \cos\alpha \sin(\phi_f - \phi_s) \quad (6)$$

where ϕ_s and ϕ_f are the azimuths of the station and the horizontal projection of the force measured clockwise from the north, respectively. Adding (4) (for a source $f_o s(t)$) and (5), we have

$$\hat{V}_r(\omega) = \frac{i r_s P_R^{(1)}}{N}\omega\hat{s}(\omega) f_o \cos\alpha\left[\xi + i\cos(\phi_f - \phi_s)\right] \quad (7)$$

$$\xi = \left[\frac{\tan\alpha}{N}\frac{y_1(r_s)}{y_3(r_s)} + \frac{N}{r_s}\frac{N_R^{(1)}}{P_R^{(1)}}\frac{\omega\hat{s}_M(\omega)M_o}{\omega\hat{s}(\omega) f_o \cos\alpha}\right] \quad (8)$$

where ξ gives the contribution of the vertical component and the isotropic component relative to that of the horizontal component of the force. In (6) and (7), the left-hand side is the observed spectrum, and the unknowns are $\omega\hat{s}(\omega) f_o \cos\alpha$, ϕ_f,

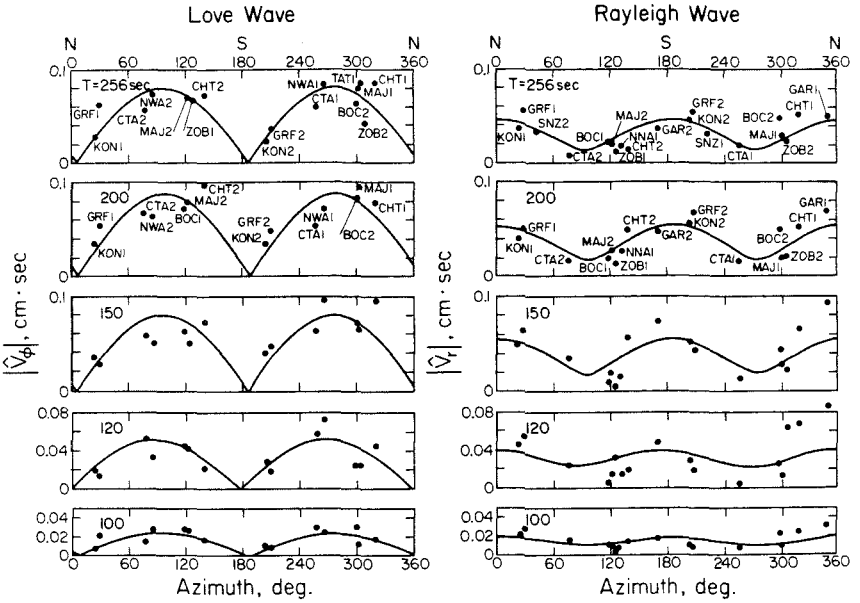

Fig. 3a.

Fig. 3. The source spectrum of the Love and Rayleigh waves $\hat{V}_r$ and $\hat{V}_\phi$ at five periods, 256, 200, 150, 120, and 100 s. The phase spectrum (Figure 3b) is obtained only for the period of 256 s. The phases used for the periods of 150, 120, and 100 s are the same as those used for the period of 200 s. The solid curves in Figure 3a are the amplitude radiation patterns determined by the least squares fit of the data. The solid, dotted, and dashed curves in Figure 3b are calculated for the solutions given in Table 2.

$\tan\alpha$, and $\hat{s}_M(\omega)M_o$. However, $\tan\alpha$ and $\hat{s}_M(\omega)M_o$ are included in ξ as a linear combination; they cannot be determined independently. Hence we treat ξ as an unknown.

Using (6) and (7), we invert the observed spectra shown in Figure 3 by using the method of least squares and determine these unknowns. Since the phase spectra are relatively poorly determined, we first invert the amplitude data only. Since (6) and (7) are nonlinear with respect to the unknowns, a first approximation is required for each one of the unknowns. On the basis of the preliminary consideration described earlier, we use $\omega\,\hat{s}(\omega)f_o\cos\alpha = 10^{18}$ dyne and $\phi_f = 180^o$, and $\xi = 0.5$. With these initial values, we perform inversion at the periods of 256, 200, 150, and 100 s and summarize the results in Table 2.

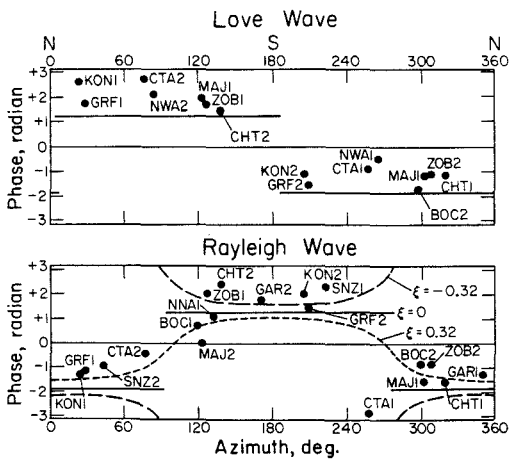

Fig. 3b.

As mentioned earlier, since M_o and α cannot be determined separately, the results are shown for two cases: (1) $M_o = 0$ (no isotropic component) and (2) $\alpha = 0$ (horizontal force).

The inversion is stable; inversion with a wide range of the initial values of the unknowns yields the same results. However, since only the amplitude data are used for inversion, ϕ_f can be only determined modulo 180^o; i.e., $\phi_f + 180^o$ yields the same fit. As shown later, the solution with $\phi_f \simeq 180^o$ is preferred on the basis of the phase data.

Table 2 shows that if $M_o = 0$, α is 12^o to 13^o except for T = 100 and 125 s where the Rayleigh wave amplitude is very small. On the other hand, if $\alpha = 0$, an isotropic source with a moment spectral density of approximately 10^{26} dyne cm s is required to explain the observed Rayleigh wave spectra. As (7) indicates, the vertical component and the isotropic component contribute to the baseline of the Rayleigh wave amplitude spectra shown in Figure 3a. In view of the noise level of the amplitude data, we consider the combined effect of these two components insignificant.

It is possible, though very unlikely, that both the vertical and the isotropic components are large, but they cancel each other, producing only insignificant amounts of overall excitation of Rayleigh waves. However, as we will show later, the absence of higher-mode Rayleigh waves with a circular radiation pattern predicted by an isotropic source eliminates this possibility.

From Table 2, we compute the amplitude spectral densities of the force, $|f_o\,\hat{s}(\omega)|$, which are shown in Figure 5. Since the phase spectrum could be obtained only at 256 s, it is not possible to determine the time history $f_o s(t)$ directly; any

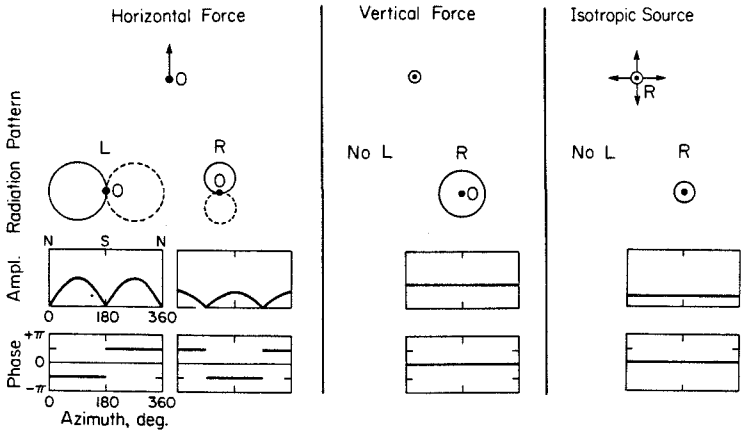

Fig. 4. Schematic diagrams showing the amplitude and the phase radiation patterns of fundamental mode Love and Rayleigh waves at T = 256 s computed for a northward horizontal force, upward vertical force, and an isotropic (explosion) source. The moment of the isotropic source is 2×10^7 cm times the magnitude of the single force. The relative amplitudes are scaled correctly. The phase spectrum shows the relative phase.

time function which explains the spectral data shown in Figure 5 is a possible candidate.

Here we try to determine an approximate form of s(t) by matching synthetic seismograms computed for a variety of s(t) with the observed seismograms. As mentioned earlier, the observed surface waves do not contain much energy at periods shorter than 75 s (Figures 1 and 2). In order to explain this feature, the source time function must be a smooth function with an effective width of approximately 75 s. Among several trial functions having a simple form, we found that a function

$$f_o s(t) = \begin{cases} 1/2\, f_o\, (1-\cos(\frac{t}{\tau}\pi)) & 0 \leqslant t \leqslant 2\tau \\ 0 & t \geqslant 2\tau \end{cases} \qquad (9)$$

can explain the observed waveforms satisfactorily. This function, whose first derivative is zero at the beginning and the end (i.e., $\dot{s}(0) = \dot{s}(2\tau) = 0$), produces smooth seismograms. The transform $f_o\hat{s}(\omega)$ is given by

$$f_o\hat{s}(\omega) = f_o\tau\left(\frac{\sin\omega\tau}{\omega\tau}\right)\frac{\pi^2}{\pi^2-(\omega\tau)^2}\, e^{-i\omega\tau} \qquad (10)$$

As shown in Figure 5, with an appropriate choice of τ, we can make the amplitude spectrum $|f_o\,\hat{s}(\omega)|$ fit the observed trend reasonably well.

We compute synthetic seismograms using (1) and (3) and, after applying an appropriate instrument response (either IDA, SRO, or ASRO), compare them with the observed seismograms at several stations, as shown in Figure 6. The onset of s(t) is placed at the origin time of the $m_b = 4.7$ earthquake. Here, we compare the overall frequency content only; no attempt is made to match the details of the waveform. As Figure 6 indicates, among the six time constants tested, $\tau = 75$ s gives the best match. This time constant also gives a correct spectral shape of the source time function, as shown in Figure 5. Also, we find that the group arrival times of the synthetic Rayleigh waves agree approximately with those of the observed. This indicates that the beginning of s(t) coincides approximately (about ±20 s) with the $m_b = 4.7$ earthquake.

TABLE 2. Results of Inversion

			Solution With $M_o = 0$		Solution With $\alpha = 0$	
T,s	ϕ_f,deg	ξ	$f_o \cdot \hat{s}(\omega)$ (10^{18}dyne-sec)	$\pm\alpha$ (deg)	$f_o \cdot \hat{s}(\omega)$ (10^{18}dyne-sec)	$M_o \hat{s}_M(\omega)$ (10^{26}dyne-cm-sec)
256	185 ± 4	0.32 ± 0.17	52.1 ± 2.8	12 ± 6	50.9 ± 2.7	5.02 ± 2.67
200	188 ± 4	0.33 ± 0.17	53.4 ± 3.1	12 ± 6	52.2 ± 3.0	3.83 ± 1.97
150	186 ± 5	0.35 ± 0.21	43.6 ± 3.4	13 ± 8	42.5 ± 3.3	2.29 ± 1.38
120	177 ± 8	0.72 ± 0.25	29.7 ± 3.6	26 ± 9	26.7 ± 3.2	2.19 ± 0.76
100	188 ± 7	0.70 ± 0.20	12.3 ± 1.2	25 ± 7	11.1 ± 1.1	0.76 ± 0.22

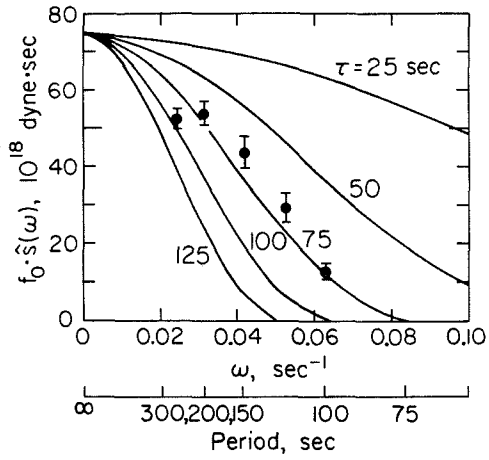

Fig. 5. The amplitude spectrum of the time function of the single force. Solid curves are computed by using equation (10).

We now use this source time function and examine the observed phase spectra at 256 s (Figure 3b). Using (10) and the values of ξ and ϕ_f listed in Table 2, we compute the source phase spectra from (6) and (7) and compare them with the data shown in Figure 3b. The calculated phases agree reasonably well with the observed. In particular, it is clear that a southward pointed force ($\phi_f = 185^\circ$) is the correct choice; if $\phi_f = 185^\circ + 180^\circ$ (northward pointed force) is used, π should be added to the calculated phases, which would cause gross disagreement between the calculated and the observed phases. Also, the calculated phases for the range of ξ from -0.32 to 0.32 are in good agreement with the data, indicating that the combined effect of the vertical component and the isotropic component is relatively unimportant.

Figure 3b indicates that the calculated phase for Love waves is systematically smaller than the observed by about 0.5 rad. If $\xi = 0$ or $\xi = 0.32$ is used, a similar trend is seen for Rayleigh waves. This difference could be explained if the starting time of s(t) is set at about 20 s before the origin time of the $m_b = 4.7$ event, or if the peak of s(t) is moved backward in time by about 20 s.

We conclude that the source time history given by s(t) with $\tau = 75 \pm 10$ s starting from the approximate origin time of the $m_b = 4.7$ earthquake gives a good approximation of the time history of the force which represents the mechanical response of the earth to the eruption. The magnitude of the force f_o can be determined from the value of $f_o \hat{s}(0) = f_o \tau$. Figure 5 gives $f_o \hat{s}(0) = 7.5 \times 10^{19}$ dyne s from which we obtain $f_o = 10^{18}$ dynes using $\tau = 75$ s. Although the spectral shape of the time function s(t) given by (9) explains the observed spectrum reasonably well, as shown by Figure 5, a slight discrepancy may be noted at the long-period end of the spectrum. The observed spectrum seems to be peaked at about 200 s ($\omega = 0.031$ s^{-1}). This discrepancy could be removed by modifying s(t), in particular, by adding an overshoot at the end thereby reducing the DC ($\omega = 0$) component of the spectrum. However, because of the limited bandwidth of the data, we could not determine the details. It is possible that the actual source process had a very long-period tail.

4. Discussion

Short-Period Events

In the analysis described above, we are concerned with only long-period characteristics of the source. The short-period behavior of the source is difficult to determine from surface waves because our knowledge of the earth's response is less accurate than at long periods. The surface wave data analyzed above is processed to remove all information at periods less than 30 s. Therefore the source time function s(t) shown in Figure 6 should be regarded as a low-pass-filtered description of the source.

Here we qualitatively discuss the short-period characteristics of the source using body waves and short-period Rayleigh waves. Inspection of the P waves recorded by SRO and ASRO stations clearly indicates two wave trains approximately 110 s apart. As an example, the SRO seismogram recorded at GRFO is shown in Figure 7 (trace c). Similar records are obtained at other stations with the separation between the two events about the same. Also, two distinct Rayleigh wave trains, about 110 s apart, are observed on the Pasadena Press-Ewing seismogram which is compared with the GRFO record in Figure 7 (trace e). Using these Rayleigh wave data and Alewine's [1972] amplitude attenuation curve for a continental crust, we obtain a surface wave magnitude of 5.3 for both events. For comparison, the long-period (T > 150 s) amplitude

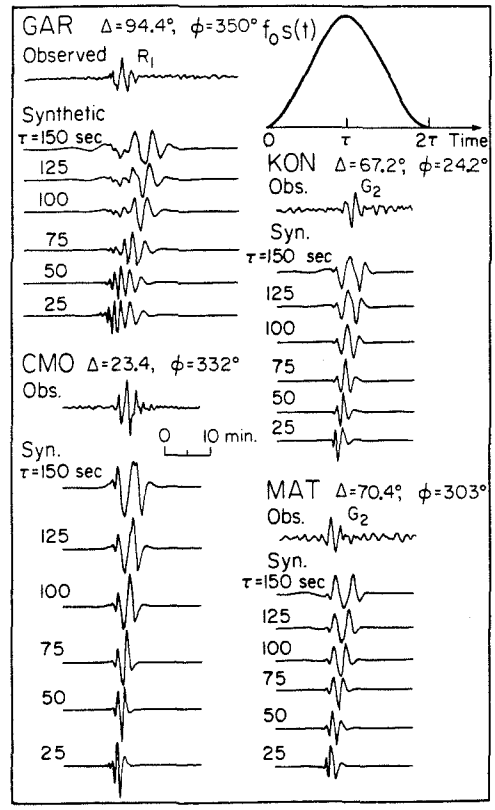

Fig. 6. Comparison of the observed seismogram and synthetic seismograms computed for source time functions with various values of τ.

spectrum of the eruption is comparable to that of the May 25, 1980, Mammoth Lakes earthquake [Given et al., 1982] (shown in Figure 2) which has M_S = 6.1 and M_W = 6.2.

Although we could not determine the mechanism of the short-period events, deconvolution (removal of the instrument response) of the GRFO record (Figure 7, trace b) reveals that two distinct events, each consisting of several pulses, are responsible for the complex wave train. The short-period, double source is reconvolved with the instrument response, and the resulting synthetic seismogram is also shown in Figure 7 (trace d). The two sources are adequate to explain the first 3 min of the body wave data.

The arrival times of the P waves from the first event are within 10 s of the arrival times expected for the m_b = 4.7 earthquake reported by NEIS (origin time: 1532:11). Malone et al. [1982] report, on the basis of local seismological data, that a second large earthquake occurred about 2 min after the first event. We take the second event on the short-period data to represent this earthquake.

On the basis of these results, we conclude that two relativaly abrupt events (mechanism unknown) occurred, one near the beginning and the other near the end of the more gradual event characterized by the bell-shaped single force $f_o s(t)$ (see traces a and b in Figure 7). After the second event, the SRO seismogram indicates a sequence of smaller events lasting at least several minutes.

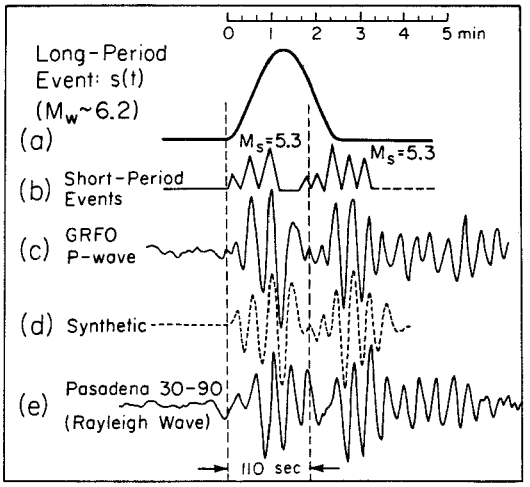

Fig. 7. P waves recorded by a long-period SRO seismograph at GRF (trace c) and short-period Rayleigh waves recorded at Pasadena (trace e). Trace b shows the source time function obtained from trace c after the instrument response is removed. The amplitude scale is arbitrary. Trace d is the synthetic computed by convolving trace b with the instrument response. The time history of the single force inferred from the long-period waves is shown for comparison (trace a).

Interpretation of the Single Force

Here we interpret the single force and the high-frequency events in terms of the various events associated with the eruption. Several pertinent observations made by various investigators are summarized in Figure 8. The time history of the source obtained above is also shown for comparison. After the m_b = 4.7 (M_S = 5.2) earthquake at 1532:11 UT on May 18, 1980, a 2.3-km^3 retrogressive rockslide on the north slope of Mount St. Helens began. Voight et al. [1982] estimate that the slide began at 7 to 20 s after the earthquake. At 1532:47 the slide had traveled about 700 m, and the velocity of the first slide block was 50 m/s and increasing [Voight et al., 1982; Glicken et al., 1981]. Pressure release caused by removal of this block resulted in hydrothermal and magmatic explosions which in turn produced a massive lateral blast.

Moore and Rice [1981] report, on the basis of measurements from infrared sensors aboard two U.S. Air Force satellites and of ground photographic and eyewitness records, that two major explosive events, each producing pyroclastic surges, occurred. The first explosion occurred at about 1532:30 and the second at about 1534, a few kilometers north of the first. The pyroclastic surge generated by the explosion moved to the north over an area of about 600 km^2 and emplaced 0.19 km^3 of surge-related deposits.

Kieffer [1981a, b] presents a steady flow model for the lateral blast. In her model, the blast was a supersonic expansion of a multiphase mixture from a disk-shaped reservoir at a pressure much greater than that of the atmosphere into which it expanded. The frontal surface of this disk (vent) is assumed to be a rectangle 1 km in east-west dimension and 0.25 km in height. Kieffer estimates that the reservoir pressure was 125 bars and half of the mass of the blast was discharged through the vent in 10 to 20 s at the initial velocity of 100 m/s. She also estimates that the pressure P*, velocity U*, and the density ρ^* at the vent are 75 bars, 104 m/s and 0.61 g/cm^3, respectively. The total mass flux at the source is then $\dot{m} = \rho^* U^* A$, where A is the area of the vent, which is 0.25 km^2. These estimates give $\dot{m} \cong 1.5 \times 10^{13}$ g/s.

We now interpret the magnitude and the time history of the single force in terms of the sequence of the events summarized above (see Figure 8). The initial event was the massive landslide which started slowly. A landslide exerts a force on the ground as it accelerates. We model a landslide by a mass M sliding down with velocity v on an inclined surface with slope γ. We let F_x and F_z be the x (horizontal) and z (vertical) components, respectively, of the force exerted by the ground on the mass. This force consists of the normal force against the load and the frictional force. The equations of motion of the mass are then $F_x = M\dot{v} \cos\gamma$ and $Mg + F_z = M\dot{v} \sin\gamma$. The force exerted by the mass on the ground is then given by

$$(-F_x) = -M\dot{v} \cos\gamma \text{ and } (-F_z) = Mg - M\dot{v} \sin\gamma$$

Since only the time dependent part of this force contributes to the generation of seismic waves, the equivalent force for the landslide is given by $f_x = -M\dot{v} \cos\gamma$ and $f_z = -M\dot{v} \sin\gamma$. Since $|f_z/f_x| = \tan\gamma$, we ignore f_z for a small $\gamma (< 20^o)$ typical of landslides. Since f_x and $\dot{v}$ have the opposite sign, a northward landslide results in a

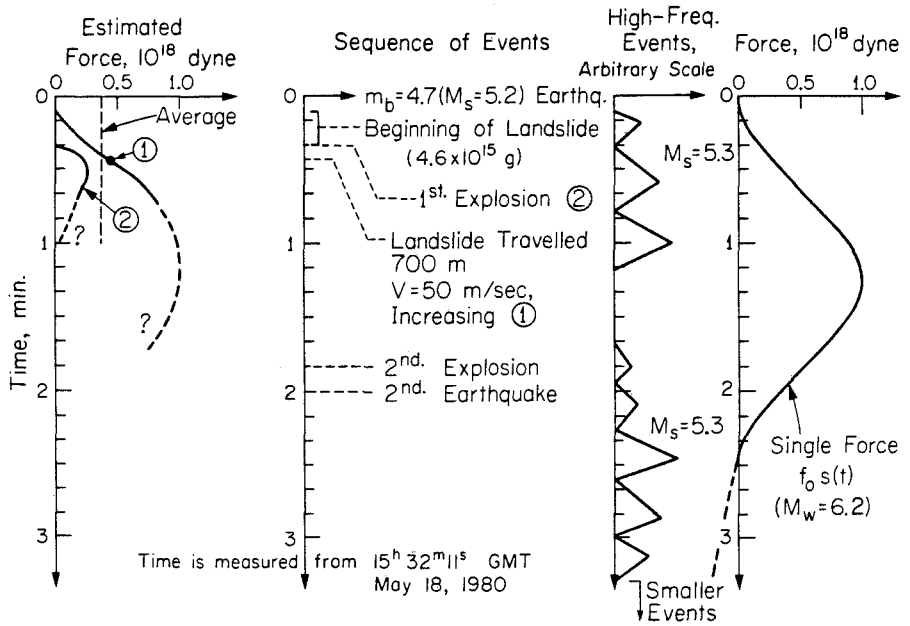

Fig. 8. Schematic diagrams showing the sequence of various events associated with the Mount St. Helens eruption. Time is taken positive downward. The time history of the single force determined from surface waves is shown on the right, and the magnitude and the time history of the force estimated from the reported sequence are shown on the left. References are Voight et al. [1982], Glicken et al. [1981], Moore [1981], Moore and Rice [1981], Malone et al. [1982], and Kieffer [1981a, b].

southward force during acceleration stage and a northward force during deceleration stage.

Using the results of Voight et al. [1982] and Glicken et al. [1981], we obtain $M = 4.6 \times 10^{15}$ g (density of the landslide mass is assumed to be 2 g/cm^3) for the Mount St. Helens landslide. Although the time history of acceleration is not known, Voight et al.'s [1982] description indicates that the average acceleration during the first minute after the $m_b = 4.7$ event is about 1 m/s^2, and the landslide was still being accelerated at the time when the lateral blast occurred (see Figure 8). This acceleration is comparable to the component of g along a slope with a grade of 6° and is reasonable for a landslide with very little friction. These estimates suggest an average magnitude of the force of approximately 4.6×10^{17} dynes. The source time history (9) gives an average force during the first minute of

$$\bar{f} = f_o \frac{1}{60} \int_0^{60} s(t)dt = 3.8 \times 10^{17} \text{ dynes}$$

which is in good agreement with the above estimate. Our time function suggests that the total force caused by the landslide was very gradual, starting from zero. This is reasonable because the landslide probably started very slowly and the entire mass did not participate in the motion simultaneously. If the landslide started from a point and propagated radially, the mass involved in the slide would increase as t^2 (t, time) so that the time history of the force would be quadratic in time. The source time function given by (9) is initially a quadratic in time. In view of the various uncertainties involved in the above estimates, we consider this agreement satisfactory and conclude that the initial stage of the landslide is the main cause of the long-period seismic excitation.

The effect of the lateral blast can be calculated by using Kieffer's [1981a, b] model. We assume that the force acting on the earth through the mountain is due to the pressure near the vent (P_v = 75 bars) and the counterforce of the blast. Since the mass flux is estimated to be $\dot{m} = 1.5 \times 10^{13}$ g/s, and the initial velocity near the vent is about $v = 100$ m/s, the latter force is about $\dot{m}v = 1.5 \times 10^{17}$ dynes. The force due to the pressure near the vent is $P_v A = 75 \times 10^6 \times 0.25 \times 10^{10}$ dyne $= 1.9 \times 10^{17}$ dynes, and the total force is then 3.4×10^{17} dynes. Actually, Kieffer [1981b] estimates that only about half of the mass was discharged at the peak steady flow velocity of 100 m/s over a period of 10 to 20 s, and the remainder followed at decreasing velocities. Therefore, the thrust of 3.4×10^{17} dynes is a maximum value, lasting perhaps for 10 to 20 s, and the thrust decreased thereafter as the mass flux and discharge velocity decreased.

Figure 8 schematically shows the time history of the force suggested by the initial landslide and the lateral blast. The beginning of the blast is set at the time of the first explosion described by Moore and Rice [1981], although it may be subject to some uncertainty. The magnitude of the calculated force agrees reasonably well with that determined from long-period seismic waves, at least during the first minute. It is interesting to compare the sequence of the high-frequency events inferred from the body wave data to the times of the earthquakes and the explosions. It is possible that the pulses of the first event correspond to the first $m_b = 4.7$ earthquake and the first explosion. Likewise, the pulses of the second event may represent the second explosion and the second earthquake. The

smaller events following the second event may represent various effects caused by the landslide during its deceleration stage and by the explosions during its terminal stage. The landslide which eventually decelerated to a halt must have caused a negative (northward) force during the later stage. Also the lateral blast must have exerted northward (and probably east and westward too) force on the ground when it blew down the trees in the area extending to a maximum distance of 28 km from the crater [Moore, 1981] and the ejecta landed again. Thus the time history of the force is expected to be very complex about 100 s or so after the beginning of the slide. As we discussed earlier, our time function represents only a gross feature and does not preclude an overshoot at the end, particularly if the overshoot had a relatively long time constant ($\geq$ 300 s).

In view of the uncertainties in the timing of the various events and the spatiotemporal patterns of the landslide and the lateral blast, more detailed comparison would not be warranted now. However, when more detailed physical models are constructed on the basis of various field observations in the future, the results obtained in this paper would be useful to constrain those models.

Seismic Radiation by a Landslide

Nakamura [1980] suggests that the 1975 Kalapana, Hawaii, earthquake (M_S = 7.1) is a result of large-scale gravitational sliding (in S20°E direction) of a land mass in the south flank of Kilauea volcano. If his interpretation is correct, this earthquake also may be modeled by a nearly horizontal force in N20°W direction. The first-motion data and the surface wave radiation patterns presented by Furumoto and Kovach [1979] and Ando [1979] are consistent with this model, although Furumoto and Kovach and Ando interpreted them by using a double-couple model. Whether or not this single-force model can explain other data as well must await further studies.

Radiated Energy at Long Period

The energy radiated into the earth's interior as very long period ($T \geq 75$ s) seismic waves can be estimated by two methods: (1) summation of normal mode energy with appropriate excitation functions as weighting functions [Kovach and Anderson, 1967; Abe, 1970], and (2) integral of energy of plane waves radiated from a point source over a spherical surface surrounding the source [Haskell, 1964]. Here, in order to obtain an order of magnitude estimate of the energy radiated from a single-force source whose time history is given by (9), we use the second method. We place a single force $f_o s(t)$ in a homogeneous whole space with density ρ, P wave velocity v_p, and S wave velocity v_s. Using equations (15) and (16) of Haskell [1964], we obtain the expressions for the energy radiated in P waves and S waves:

$$E_P = \frac{f_o^2}{12\pi\rho v_p^3} \int_{-\infty}^{+\infty} \dot{s}(t)^2 dt \qquad (11)$$

and

$$E_s = \frac{f_o^2}{6\pi\rho v_s^3} \int_{-\infty}^{+\infty} \dot{s}(t)^2 dt \qquad (12)$$

Substituting $\dot{s}(t) = \frac{\pi}{2\tau} \sin(\frac{t}{\tau}\pi)$, we have

$$E_s = \frac{\pi}{24} \frac{f_o^2}{\rho v_s^3 \tau} = 1.6 \times 10^{16} \text{ ergs}$$

and

$$E_p = 0.096\ E_s = 1.5 \times 10^{15} \text{ ergs}$$

where ρ = 2.6 g/cm^3, v_s = 3.5 km/s, $v_p/v_s = \sqrt{3}$, τ = 75 s, and $f_o = 10^{18}$ dynes. Thus the total radiated energy in a period range longer than 75 s is $E = E_s + E_p = 1.8 \times 10^{16}$ ergs, which corresponds to the energy released in an ordinary (tectonic) earthquake of $M_s \cong 3$. This is substantially smaller than the magnitude of numerous local earthquakes which occurred in association with the eruption [Malone et al. 1982].

Kieffer [1981a] estimates the energy released during the propagation of the blast to be 3×10^{23} ergs. The potential energy released by the landslide is estimated to be approximately 5×10^{23} ergs, if $M = 4.6 \times 10^{15}$ g and an average drop of 1 km are used. Bolt and Tanimoto [1981] estimate that the energy carried by the atmospheric waves is at least 10^{22} ergs. The surface wave magnitude of the earthquake associated with the eruption is 5.2, which suggests that the energy radiated in short-period seismic waves is about 2×10^{19} ergs if the standard magnitude-energy relation [Gutenberg and Richter, 1956] is used.

Thus, the energy coupled to the ground at periods longer than 75 s is only 0.1%, 2×10^{-6}, and 2×10^{-8} of the total elastic wave energy, the energy carried by the atmospheric waves, and the total energy released in the eruption, respectively.

Magnitude of the Isotropic Component

As was discussed earlier, we cannot estimate the magnitude of the vertical force and the isotropic source separately by using fundamental modes only. Here we show that combined use of fundamental and higher modes can constrain the magnitude of the isotropic component. From (8) we obtain the ratio η of the excitation due to an isotropic source to that due to a vertical force as

$$\eta = \left| \frac{N M_o}{r_o f_o} \frac{\hat{s}_M(\omega)}{\hat{s}(\omega)} \left(\frac{N y_3(r_s)}{y_1(r_s)} \right) \frac{N_R^{(1)}}{P_R^{(1)}} \right|$$

Since $|N_R^{(1)}/P_R^{(1)}| \simeq 3/2$ for a shallow source, η is proportional to $|Ny_3(r_s)/y_1(r_s)|$. At the period range of our interest (100 to 200 s), $|Ny_3(r_s)/y_1(r_s)| \simeq 0.7$ and 2 to 3 for fundamental modes and higher-mode Rayleigh waves, respectively. Hence, $|\eta_{\text{higher modes}}/\eta_{\text{fundamental mode}}|$ is approximately 3 to 4. Thus an isotropic source is far more efficient than a vertical force in the excitation of higher-mode Rayleigh waves

relative to fundamental modes. Hence, existence of an isotropic source would produce a circular (azimuth independent) radiation pattern of higher-mode Rayleigh waves.

As shown by Figure 1, higher-mode Rayleigh waves were observed at some stations (e.g., KON) but not at every station (e.g., MAJ). We find that the radiation pattern of the higher modes is essentially similar to that of the fundamental modes, suggesting that there is no significant contribution from an isotropic source. In fact, the amplitudes of the observed higher modes are consistent with those predicted by the estimated horizontal force. We therefore conclude that the contribution from the isotropic source is negligible.

'Single Force'

Although we conclude that a single force is the most adequate kinematic representation of the eruption of Mount St. Helens, we do not mean that a single force was actually applied at the source. Any physical source within the earth atmosphere system must be represented by a force system with vanishing total force and moment. In case of the landslide and the lateral blast associated with the Mount St. Helens eruption, only such forces which were exerted on the solid part of the earth within a time period of several minutes after the eruptions were detected by the global seismographic networks. The single force discussed in this paper represents the overall effect of these forces.

5. Conclusion

The amplitude radiation patterns of both Rayleigh and Love waves excited by the eruption of Mount St. Helens of May 18, 1980, are two lobed with a nodal direction in E5°S for Rayleigh waves and in N5°E for Love waves. These radiation patterns preclude any double-couple mechanism. The radiation pattern, the initial phase, the relatively large amplitude ratio of Love to Rayleigh waves, and the existence of clear nodes in the radiation patterns of fundamental and higher-mode Rayleigh waves suggest that the source is represented by an almost horizontal (less than 15° from the horizontal) single force pointed toward S5°W. The surface wave spectra fall off very rapidly at periods shorter than 75 s, suggesting a very slow source process. Although the details of the source time history could not be determined, a smooth bell-shaped time function

$$f_o s(t) = \begin{cases} (1/2) f_o (1-\cos(\frac{t}{\tau}\pi)) & 0 \leq t \leq 2\tau \\ 0 & t \geq 2\tau \end{cases}$$

with τ = 75 s is considered appropriate on the basis of comparison between synthetic and observed seismograms and of the shape of the source spectrum. The peak value of the force f_o is about 10^{18} dynes. The tailing end of the source time function could not be resolved, and some overshoot may be added. The magnitude and the time history of the force can be explained by a northward landslide followed by a lateral blast.

Acknowledgments. We thank all the participants in the coffee break at the Seismological Laboratory. Their enthusiasm and interest prompted us toward completion of this study. In particular, the last part of this paper was written on the basis of discussions during the numerous coffee breaks and on some detailed notes on rocket propulsion and inclined plane handed to us later by Don Anderson, Brad Hager, and Tom Heaton. Sue Kieffer and Kazuaki Nakamura made very helpful suggestions on the mechanism of lateral blast and landslide respectively. We thank Harry Glicken, Stephen Malone and James Moore for useful information on the sequence of the various events. Emile Okal and Sue Kieffer reviewed the manuscript and made helpful comments. The IDA data were made available to us by courtesy of the IDA Project team at the University of California, San Diego, and the SRO and ASRO data were provided by the U.S. Geological Survey. Research supported by the U.S. Geological Survey contract 14-08-0001-19755, National Aeronautics and Space Administration grant NSG-7610, and National Science Foundation grant EAR78-11973. Contribution 3708, Division of Geological and Planetary Sciences, California Institute of Technology, Pasadena, California, 91125.

References

Abe, K., Determination of seismic moment and energy from the earth's free oscillation, Phys. Earth Planet. Inter., 4, 49-61, 1970.

Alewine, R. W., III, Theoretical and observed distance corrections for Rayleigh-wave magnitude, Bull. Seismol. Soc. Am., 62, 1611-1619, 1972.

Ando, M., The Hawaii earthquake of November 29, 1975: Low dip angle faulting due to forceful injection of magma, J. Geophys. Res., 84, 7616-7626, 1979.

Bolt, B. A., and T. Tanimoto, Atmosphere oscillations after the May 18, 1980 eruption of Mount St. Helens, Eos Trans. AGU, 62, 529-530, 1981.

Furumoto, A. S., and R. L. Kovach, The Kalapana earthquake of November 29, 1975: An intra-plate earthquake and its relation to geothermal processes, Phys. Earth Planet. Inter., 18, 197-208, 1979.

Given, J. W., T. C. Wallace, and H. Kanamori, Teleseismic analysis of the 1980 Mammoth Lakes earthquake sequence, Bull. Seismol. Soc. Am., in press, 1982.

Glicken, H., B. Voight, and R. J. Janda, Rockslide-debris avalanche of May 18, 1980, Mount St. Helens volcano, paper presented at the IAVCEI (International Association of Volcanology and Chemistry of the Earth's Interior) Symposium, Tokyo, Aug. 28-Sept. 9, 1981.

Gutenberg, B., and C. F. Richter, Magnitude and energy of earthquakes, Ann. Geofis., 9, 1-15, 1956.

Haskell, N. A., Total energy spectral density of elastic wave radiation from propagating faults, Bull. Seismol. Soc. Am., 54, 1811-1841, 1964.

Kanamori, H., Synthesis of long-period surface waves and its application to earthquake source studies--Kurile islands earthquake of October 13, 1963, J. Geophys. Res., 75, 5011-5027, 1970.

Kanamori, H., and J. J. Cipar, Focal process of the great Chilean earthquake, May 22, 1960, Phys. Earth Planet. Inter., 9, 128-136, 1974.

Kanamori, H., and J. W. Given, Use of long-period surface waves for fast determination of earthquake source parameters, Phys. Earth Planet. Inter., 27, 8-31, 1981.

Kanamori, H., and G. S. Stewart, Mode of the strain release along the Gibbs fracture zone, Mid-Atlantic Ridge, Phys. Earth Planet. Inter., 11, 312-332, 1976.

Kieffer, S. W., Blast dynamics at Mount St. Helens on 18 May 1980, Nature, 291, 568-570, 1981a.

Kieffer, S. W., The lateral blast of May 18 at Mount St. Helens, paper presented at the IAVCEI (International Association of Volcanology and Chemistry of the Earth's Interior) Symposium, Tokyo, Aug. 28-Sept. 9, 1981b.

Kovach, R. L., and D. L. Anderson, Study of the energy of the free oscillations of the earth, J. Geophys. Res., 72, 2155-2168, 1967.

Malone, S. D., E. Endo, C. S. Weaver, and J. W. Ramey, Seismic monitoring for eruption prediction, The 1980 Eruptions of Mt. St. Helens, U.S. Geol. Surv. Prof. Pap., 1250, 803-813, 1982.

Moore, J. G., The pyroclastic surge of May 18, 1980, Mt. St. Helens, Washington, paper presented at the IAVCEI (International Association of Volcanology and Chemistry of the Earth's Interior) Symposium, Tokyo, Aug. 28-Sept. 9, 1981.

Moore, J. G., and C. J. Rice, Chronology and character of Mt. St. Helens explosive eruptive phase of May 18, 1980, (abstract), Eos Trans. AGU, 62, 1081, 1981.

Nakamura, K., Why do long rift zones develop in Hawaiian volcanoes, in Japanese, Kazan, 25, 255-269, 1980.

Okal, E. A., A physical classification of the earth's spheroidal modes, J. Phys. Earth, 26, 75-103, 1978.

Saito, M., Excitation of free oscillations and surface waves by a point source in a vertically heterogeneous earth, J. Geophys. Res., 72, 3689-3699, 1967.

Voight, B., H. Glicken, R. J. Janda, and P. M. Douglass, Catastrophic rockslide-avalanche of May 18, The 1980 Eruptions of Mount St. Helens, U.S. Geol. Surv. Prof. Pap., 1250, 347-378, 1982.

(Received October 15, 1981;
revised March 2, 1982;
accepted March 12, 1982).